Solution Structure of Oxidized Cytochrome c_6 from the Green Alga *Monoraphidium braunii*[†,‡]

Lucia Banci,[§] Ivano Bertini,*[,§] Miguel A. De la Rosa,[||] Dionysios Koulougliotis,[§] José A. Navarro,[||] and Olaf Walter[§]

Department of Chemistry, University of Florence, Florence, Italy, and Instituto de Bioquímica Vegetal y Fotosíntesis, Universidad de Sevilla y CSIC, Sevilla, Spain

Received November 10, 1997; Revised Manuscript Received January 19, 1998

ABSTRACT: Cytochrome c_6 from *Monoraphidium braunii*, an 89-amino acid electron transfer protein, has been investigated by NMR in solution, in its oxidized form, at pH 7 and 300 K. By using a combination of COSY, TOCSY, and NOESY experiments, 84% of the proton resonances have been assigned. A total of 1668 experimental NOE constraints, 1109 of which were meaningful, together with 288 pseudocontact shifts, have been used to determine the structure in solution. This is represented as a family of 40 structures which have been energy minimized. The rmsd values with respect to the mean structure are 0.57 ± 0.08 and 0.94 ± 0.09 Å for the backbone and heavy atoms, respectively. The structure has been found to be very similar to that of the reduced form, except for a rearrangement in propionate 7, a feature which has been observed in all *c*-type cytochromes investigated so far. Such a feature could be relevant for the efficiency of the electron transfer pathway with either the oxidizing or the reducing partners. Other differences in the oxidation states have been noted in the region proposed to be involved in the interaction with the physiological partners.

The structural changes occurring upon electron transfer in electron transfer proteins is the object of an international scientific debate (*1*−*3*). These possible structural changes would be relevant in determining the reorganizational energy associated with the change of the oxidation state.

Among the electron transfer proteins, the solution structures of the oxidized and reduced forms of high-potential iron−sulfur proteins (HiPIPs) have shown that, at the present level of resolution, apparently no difference is present for the two oxidation states (*4*−*7*).

At variance with this, the crystal structures of some oxidized and reduced cytochromes have shown some changes (*2*, *8*−*10*). The largest change involves the orientation of propionate 7, while minor conformational changes occur in the orientation of the axial histidine and the puckering of the heme ring. Furthermore, a change in the position of a structurally ordered water molecule close to the iron has been observed (*2*, *11*).

The solution (*12*, *13*) and crystal (*2*, *8*) structures of yeast cytochrome *c* in both its reduced and oxidized forms have shown a reorientation of propionate 7 upon the oxidation state changing. Furthermore, it has been noted that in yeast cytochrome *c* the number of backbone NH protons exchanging with D_2O as the solvent is larger in the oxidized than in the reduced form. This behavior has been discussed in terms of structural mobility, which is higher in the oxidized state, involving the two loops supporting the methionine and histidine ligands, respectively (*13*). The solution structures of oxidized (*14*, *15*) and reduced (*16*) horse heart cytochrome *c* are also available and show differences such as the orientation of the propionates.

We have extended the study to the solution structure of the oxidized and reduced forms to cytochrome c_6 (cyt c_6)[1] from the photosynthetic green alga *Monoraphidium braunii* (*17*). Like all *c*-type cytochromes, cyt c_6 contains a heme *c* moiety with the iron ion axially coordinated by a histidine and a methionine (*18*, *19*). At variance with the horse heart and yeast cytochromes *c* which are positively charged, cyt c_6 is negatively charged. The protein is characterized by a positive reduction potential (358 mV at pH 7).

The 3D structure of the reduced form of cyt c_6 is available in both solution (*18*) and the solid state (*19*). The oxidized form of cyt c_6 is quite unstable, but it could be kept in solution long enough to allow the determination of its structure by NMR spectroscopy, which is the subject of this

[†] Funded by the European Union Network (Contract CHRX-CT94-0540), E.U. Large Scale Facility Contract ERB4050PL931088, the CNR-Comitato Nazionale Biotecnologia e Biologia Moleculare (Contract 95.02860.CT14), and the Dirección General de Investigación Científica y Técnica (Grant PB93-0922). D.K. and O.W. are recipients of TMR postodoctoral fellowships (Contracts ERBFMBICT960994 and ERBFMBICT950374, respectively).

[‡] The structure coordinates have been deposited at the Brookhaven Protein Data Bank (ID code 1a2s).

* Author to whom correspondence should be addressed: Department of Chemistry, Laboratory of Inorganic and Bioinorganic Chemistry, Via G. Capponi 7, 50121 Florence, Italy. Phone: 39-55-2757539. Fax: 39-55-2757555. E-mail: bertini@risc1.lrm.fi.cnr.it.

[§] University of Florence.

[||] Universidad de Sevilla y CSIC.

[1] Abbreviations: cyt c_6, cytochrome c_6; COSY, correlated spectroscopy; DSS, 2,2-dimethyl-2-silapentane-5-sulfonate; NMR, nuclear magnetic resonance; NOE, nuclear Overhauser effect; NOESY, nuclear Overhauser effect spectroscopy; ppm, parts per million; rmsd, root-mean-squared deviation; TOCSY, total correlation spectroscopy; TPPI, time-proportional phase incrementation; WATERGATE, water suppression by gradient-tailored excitation; WEFT; water-eliminated Fourier transform; 1-, 2-, and 3D, one-, two-, and three-dimensional.

S0006-2960(97)02765-7 CCC: $15.00
Published on Web 03/17/1998

paper. Also for cyt c_6, propionate 7 shows a change in the conformation when passing from the reduced to the oxidized form, although different from that observed in other *c*-type cytochromes.

MATERIALS AND METHODS

Sample Preparation. Cytochrome c_6 from *M. braunii* (cyt c_6) was prepared and purified as previously reported (*17*). Samples for ^{1}H NMR spectroscopy were prepared in 10 mM phosphate buffer (in 90% H_2O/10% D_2O or in 100% D_2O) at pH 5, adjusted by addition of small volumes of a concentrated solution of NaOH. The final protein concentration was approximately 2.5 mM. NaN_3 was added to the samples to a concentration of 10 μM to prevent the growth of bacteria. Cytochrome c_6 has a relatively high reduction potential [358 mV at pH 7 (*17*)] and thus tends to autoreduce. Oxidation of cytochrome c_6 was achieved by addition of stoichiometric amounts of potassium ferricyanide [$K_3Fe(CN)_6$]. Thus, high-quality 2D NMR spectra were obtained. Use of degassed buffers and periodic addition (every 2−3 days) of small (substoichiometric) quantities of $K_3Fe(CN)_6$ kept the majority of the sample (90−95%) in the oxidized form. The reduced form of cytochrome c_6 in 10 mM phosphate buffer at pH 5.0 was achieved by the stoichiometric anaerobic addition of sodium dithionite. The latter was added as a small aliquot taken from a concentrated (0.25 M) degassed solution in 10 mM phosphate at pH 5.

NMR Spectroscopy. ^{1}H NMR spectra were recorded on DRX 500, AMX 600, and AVANCE 800 Bruker spectrometers, operating at nominal frequencies of 500.13, 600.13, and 800.13 MHz, respectively. 2D TPPI NOESY (*20*, *21*) and clean TOCSY (*22*, *23*) spectra were recorded with presaturation of the solvent signal during the relaxation delay (500 ms, in TOCSY and NOESY) and the mixing time (in NOESY). These maps were acquired at 300 and 295 K in D_2O and in H_2O (90% H_2O/10% D_2O). In the maps collected for the optimization of the detection of connectivities in the diamagnetic region, the spectral width was set to 40 ppm (on the Bruker AMX 600 spectrometer) or 18 ppm (on the Bruker DRX 500 or the AVANCE 800 spectrometer) and the recycle time to 600 ms. In those maps collected for the detection of connectivities between paramagnetic signals, the spectral width was set to 70 ppm and the recycle time to 300 ms. NOESY spectra were acquired with mixing times of 100 ms (for the "diamagnetic" spectra) and 25 ms (for the "paramagnetic" spectra). TOCSY maps with spin lock times of 60 and 90 ms were acquired to detect connectivities between diamagnetic signals. A phase sensitive TPPI COSY (*24*, *25*) map was recorded in a H_2O solution at 300 K. Using the WATERGATE (*26*) pulse sequence for water suppression, NOESY maps were collected on the DRX 500 and the AVANCE 800 spectrometers at a temperature of 300 K with a mixing time of 100 ms and a spectral width of 18 ppm. A superWEFT TOCSY spectrum in H_2O, with a spin lock time of 10 ms, was also acquired to enhance the sensitivity for cross-peaks between fast relaxing protons of the residues located in the vicinity of the heme.

1D NOE experiments were carried out at 500 MHz. They were performed with the superWEFT pulse sequence for water signal suppression by using the methodology already reported (*27*−*29*).

All the 2D spectra consisted of 2K data points in the F_2 dimension, while 512−900 experiments were recorded in the F_1 dimension, using 128 or 256 scans/experiment. Raw data were multiplied in both dimensions by a pure cosine-squared (NOESY and TOCSY) and a pure sine-squared (COSY) bell window function and Fourier transformed to obtain 2048 × 1024 real data points. A polynomial baseline correction was applied in both directions. The spectra were calibrated by assuming a chemical shift of 4.787 and 4.849 ppm for the water signal with respect to DSS at 300 and 295 K, respectively. Data processing was performed using a standard Bruker software package. The 2D spectra were analyzed on IBM RISC 6000 computers using the program XEASY (ETH, Zurich) (*30*).

Structure Calculations. The volumes of the assigned NOESY cross-peaks were obtained using the integration routines available in the program XEASY. The majority of the dipolar connectivities was obtained from the NOESY cross-peaks present in the WATERGATE NOESY spectrum acquired at 500 MHz at 300 K with a mixing time of 100 ms and a spectral width of 18 ppm. However, most of the dipolar connectivities involving the protons of the heme group were taken from two NOESY maps acquired in D_2O with mixing times of either 25 or 100 ms.

The approach we have used to convert NOE intensities into distances is that provided by the program CALIBA (*31*) which divides the NOEs into five different classes of distances between single protons. Five separate classes apply also for distances involving methyls, thus taking into account the three-proton degeneracy. The classification used in this work is the same as that previously reported (*30*−*33*) and holds as follows: (i) intraresidue except NH, Hα, and Hβ; (ii) sequential and intraresidue NH, Hα, and Hβ; (iii) medium-range (all nonsequential interresidue connectivities between NH, Hα, and Hβ within a segment of five consecutive residues); (iv) long-range backbone; and (v) long-range.

For each of the three integrated 2D NOESY maps, a separate run of CALIBA was performed. For the two NOESY maps collected with the same mixing time (i.e., 100 ms in either H_2O or D_2O), scaling of the volumes was done by referring to a few intraresidue connectivities whose volumes could be accurately measured in both spectra. The paramagnetic NOESY map, obtained with a 25 ms mixing time, was calibrated independently, by using a few intraresidue heme NOESY cross-peaks (e.g., α-meso proton to 2-Hα proton, α-meso to 3-CH_3, and δ-meso to 1-CH_3) known to correspond to a fixed distance, as a starting point for the calibration of the cross-peaks corresponding to protons very close to the paramagnetic center. In the following cycles of calibration, the same procedure as outlined above was used. The resulting upper distance limits are not affected by the proton pairs used in the first cycle of CALIBA as a starting point for calibration. In fact, if instead of taking the intraresidue heme NOESY cross-peaks we take as a starting point the intraresidue cross-peaks arising from the ring of Trp64 (also present in the paramagnetic NOESY map), the same upper distance limits are obtained. In addition, we should note that for those paramagnetic protons that were present in both NOESY maps (i.e., taken with 25 and 100 ms mixing times) calibration of their cross-peak experimental intensity gave very similar upper distance limits after

successive runs of CALIBA. 1D NOEs involving paramagnetic signals (for a total of 11 NOEs) were converted into upper distance limits of 5.0 Å for proton pairs involving single proton resonances.

The oxidized form of cytochrome c_6 examined here is paramagnetic, and thus, the NOE volumes corresponding to dipolar connectivities of protons located close to the heme are reduced by the effect of paramagnetism on their nuclear relaxation rates. Therefore, by ignoring the paramagnetic effect, the program CALIBA produces a relatively loose upper distance limit for paramagnetically relaxed protons. This fact may result in a less well defined structure around the paramagnetic center since the upper distance limits imposed are overestimated. However, in this structure determination, despite the loose calibration employed for some of the protons, the average total, as well as the "per residue" rmsd values, for both backbone and heavy atoms turns out to be very low (vide infra) even around the heme and even at the level of the DYANA calculations (i.e., before the introduction of pseudocontact shifts and before restrained energy minimization) (see Results and Discussion for complete presentation). It is very important to note that, at the end of the calculations, the structure is very well defined and there are no violations of the experimental NOE constraints (input in the form of upper distance limits).

Nevertheless, the effect of paramagnetism on the NOE intensities can be accounted for by a suitably modified complete relaxation matrix approach (*34*). In the case examined in ref *34* (reduced HiPIP I from *Ectothiorhodospira halophila*), accounting for the paramagnetism resulted in a decrease of the average backbone and heavy atom rmsds of approximately 0.2 Å in the vicinity of the paramagnetic center and reached, within experimental error, values as low as the ones obtained for the present system, where no correction for the paramagnetism has been employed. It should be noted that reduced HiPIP I is a small (73-residue) protein containing four Fe metal ions, and thus, the paramagnetic effect is very pronounced. Oxidized cyt c_6 is a low-spin Fe(III) monoheme 89-residue protein where the paramagnetic effect is expected to be smaller. Recently, a comprehensive review has appeared describing in more detail the above-mentioned as well as several other issues involved in the solution structure determination of paramagnetic metalloproteins (*35*).[2]

The heme was included in the structure calculations through the addition of an artificial amino acid to the standard residue library in a way similar to that previously described (*36*). This artificial residue consists of a histidine residue, whose Nϵ2 was connected to the heme skeleton through links with the four pyrrole nitrogens (upper distance limits of 2.9 Å). The heme iron was defined as a dummy atom, and its hexacoordinate geometry was realized by imposing the appropriate upper and lower distance limits between this dummy atom and the ligand atoms by "special covalent bonds" (links). Upper (2.1 Å) and lower (1.9 Å) distance limits between the cysteine sulfur and the α-carbon of the corresponding heme thioether substituent were applied to link the heme moiety to the bound cysteine. A link between Met61 and the heme iron was placed with upper and lower distance limits of 2.45 and 2.25 Å between the sulfur methionine atom and the iron atom and of 2.9 and 3.2 Å between the sulfur methionine atom and the four pyrrole nitrogens. After the appropriate bonds were defined as rotable, the heme substituents were allowed to assume all possible conformations. Analogously, the His19 ring and the Met61 side chain can change their orientations with respect to the heme plane axes.

With the preliminary structures available from the program DYANA (i.e., by taking into account only the experimental distance constraints and not including the pseudocontact shifts), the scaling factors for the volume-to-distance conversion for each class were evaluated by plotting volumes of peaks arising from pairs of protons at a fixed distance. As the structure emerged from successive runs of DYANA, selected interatomic distances were taken from these structures and additional calibrations were performed. Several cycles of the structure calculations were carried out in order to recalibrate the NOE distance constraints. At this stage, new NOESY cross-peaks have been assigned by using the program CORMA (*37*). This program is based on relaxation matrix calculations which therefore allow us to back calculate from the structure the expected NOEs between each proton pair. A single correlation time, set to 4 ns, was used. These calculations were performed on an already quite well defined family of 20 structures (see Results and Discussion). In our approach, the program CORMA uses as input the assignment of the proton chemical shifts that already has been performed "manually" by following the methods described in Results and Discussion. The new NOESY cross-peaks found by CORMA amounted to 9% of the total number of cross-peaks used as input in CALIBA.

Stereospecific assignments of diastereotopic protons and methyl groups were obtained using the program GLOMSA (*31*).

Experimental pseudocontact shifts were also used as further structural constraints. These calculations can be performed with the modified version of the DYANA program (called PSEUDYANA) (*15*, *38*) which includes the pseudocontact shift values as structural constraints. The latter contribution to the shift arises from the magnetic susceptibility anisotropy of the metal ion and depends on the position of a given nucleus with respect to the principal axes of the magnetic susceptibility tensor. It is usually described by the following equation (*39*, *40*):

$$\delta_{pc} = \frac{1}{12\pi r_i^3}[\Delta\chi_{ax}(3n_i^2 - 1) + {}^3/_2\Delta\chi_{rh}(l_i^2 - m_i^2)] \quad (1)$$

where $\Delta\chi_{ax}$ and $\Delta\chi_{rh}$ are the axial and the rhombic anisotropy of the magnetic susceptibility induced by the paramagnetic ion, respectively, r_i is the distance of the nucleus *i* from the

[2] By following the procedure described in Bertini et al. (*34*), we conducted a CORMA calculation in the present system in order to quantify the order of magnitude of the paramagnetic effects on the NOE intensities in oxidized cyt c_6. Assuming an electronic correlation time for the low-spin Fe(III) equal to 6×10^{-12} s, the calculation resulted in an average correction for five observed experimental NOE intensities, by a factor of 2.8 ± 0.5 corresponding to an overestimation of their upper distance limits, in the absence of paramagnetic correction, by $19 \pm 1\%$. For the rest of the protons located in the vicinity of the heme, an average correction factor of 1.6 ± 0.3 was calculated, corresponding to a less than 10% overestimation of their corresponding upper distance limits. The results of these test CORMA calculations strongly indicate that, for the system examined here, the error introduced to the NOE calibration due to paramagnetism is quite small.

metal ion, and l_i, m_i, and n_i are the direction cosines of the position vector of atom i ($\mathbf{r}_i$) with respect to the orthogonal reference system formed by the principal axes of the magnetic susceptibility tensor.

The resonances of Cys15 and -18, of His19, and of Met61 have not been included in the calculations as their shifts could also contain the contact contribution.

The parameters of an average magnetic susceptibility tensor have been determined by fitting a series of eq 1, each relative to one structure of the family, to the same set of experimental pseudocontact shift values, through the program FANTASIA (*41*, *42*).

The pseudocontact shifts were included as constraints in the structural calculations by minimizing the following equation for the pseudocontact shift target function:

$$t^{pc} = \sum_i k_i[\max(|\delta_{i_{calc}}{}^{pc} - \delta_{i_{obs}}{}^{pc}| - T_i,0)]^2 \qquad (2)$$

where k_i is the weight of the ith constraint (all taken equal in this work) and T_i is the tolerance on the experimental pseudocontact shift values. This tolerance measures the error with respect to the actual value. In the present calculations, the tolerance was set to 10% of the experimental shift value, with the minimum value of 0.3 ppm for the nonexchangeable protons and 0.6 ppm for the exchangeable ones. The proportionality between tolerance and pseudocontact shifts takes into account possible partial failures of eq 1 which is strictly valid only in the point dipole−point dipole approximation.

During the structure calculations, according to the procedure developed for PSEUDYANA calculations (*15*, *38*), the program looks for the best orientation and origin of the tensor that minimizes the deviation between experimental and calculated pseudocontact shifts. PSEUDYANA follows a procedure equivalent to the one used by the program PSEUDIANA (*41*) which preceded it. Sample calculations were also performed by using PSEUDIANA and gave similar results for the values of the magnetic susceptibility anisotropy parameters as well as for the tensor orientation. An important note should be made at this point: The PSEUDYANA protocol (in contrast to the one followed by PSEUDIANA) needs only the initial values (see next paragraph) of the magnetic susceptibility tensor anisotropies and not its direction cosines, i.e. no specific initial orientation is provided for the tensor. By using the simulated annealing protocol (in an equivalent manner as implemented in DYANA), it allows for a complete search in the conformational space and produces a new family of structures starting from random coils. As also discussed in the PSEUDYANA procedure (*15*, *38*), a special residue formed by dummy atoms was used to define the position of the metal center and the directions of the magnetic susceptibility tensor in the dihedral angle coordinate space. The dummy atoms of this residue have the van der Waals radius set to zero so that they can freely penetrate the molecule. An upper distance limit of 0.2 Å was set between the pseudoatom defining the metal ion and the iron ion. The location of this residue and the tensor orientation were optimized during the structural calculations.

The initial magnetic susceptibility anisotropy parameters were determined by fitting the experimental pseudocontact shifts to eq 1 using as a starting structure the family of 40 structures obtained with the DYANA calculations. The magnetic susceptibility tensor anisotropies were reevaluated after each PSEUDYANA run (a total of 6 runs was performed) and used in the following calculations. The final values of the magnetic susceptibility anisotropies ($\Delta\chi$s) vary approximately 10% (and not more than 5% after the first two cycles) compared to the ones used initially as input. Test runs were performed by using initial values for both $\Delta\chi$s 50−70% different from the ones calculated by FANTASIA. After the first PSEUDYANA calculation, they converged to values not more than 15% different from the output of FANTASIA.

The final PSEUDYANA calculations were performed by using 12 000 steps of annealing and creating 300 random structures. Of these, at least 50 resulted with total target function of less than 5 Å^2.

Structural refinement was performed with restrained energy minimization (REM) calculations performed with the SANDER module (*43*) of the AMBER software package (*44*). The pseudocontact shifts were included as contraints in a modified SANDER module, called PSEUDOREM/PSEUMD (*42*). The family of 40 structures obtained with the PSEUDYANA calculations were used as input for the PSEUDOREM calculations. The force field parameters for the heme and its ligands, as well as the overall calculation procedure, were set up as previously reported for similar systems (*13*, *18*). The initial values of the magnetic susceptibility anisotropy parameters used as input by PSEUDOREM were the output of the PSEUDYANA runs. After the end of the PSEUDOREM runs, they were subjected to a less than 3% change from their initial values.

Structure Analysis. The structure analysis, in terms of Ramachandran plots, deviation from ideal structural parameters, secondary structure elements, etc., was performed by using the program PROCHECK (*45*). Visual inspection and drawing of the various families were performed with the programs RASMOL (*46*) and MOLMOL (*47*). The calculations were performed on an IBM SP02 parallel computer.

RESULTS AND DISCUSSION

Sequence-Specific Assignment

The 2D ^{1}H NMR spectra have been recorded at both 500 and 800 MHz at 300 K and pH 5.0. The 800 MHz NMR spectra were better resolved, but contained essentially the same number of cross-peaks under the present experimental conditions. Thus, the 2D map at 800 MHz helped in the assignment process (especially for confirmation) but was not used for the cross-peak integration. The 1D NOE difference NMR spectra were recorded at 600 MHz, saturating broad NMR signals due to the axial heme ligands and/or heme substituents and detecting NOEs with signals under the diamagnetic envelope characterized by longer T_1 values (*27*−*29*).

The assignment has been performed first by the identification of the spin patterns of the side chains through the analysis of the TOCSY maps in D_2O and H_2O (taken either with presaturation of the water signal or by using the WATERGATE pulse sequence) and the COSY map in H_2O. Sequence-specific assignment was then performed by analyzing the NOESY spectra, looking for the NH−Hα and NH−NH connectivities. Sequential stretches of backbone

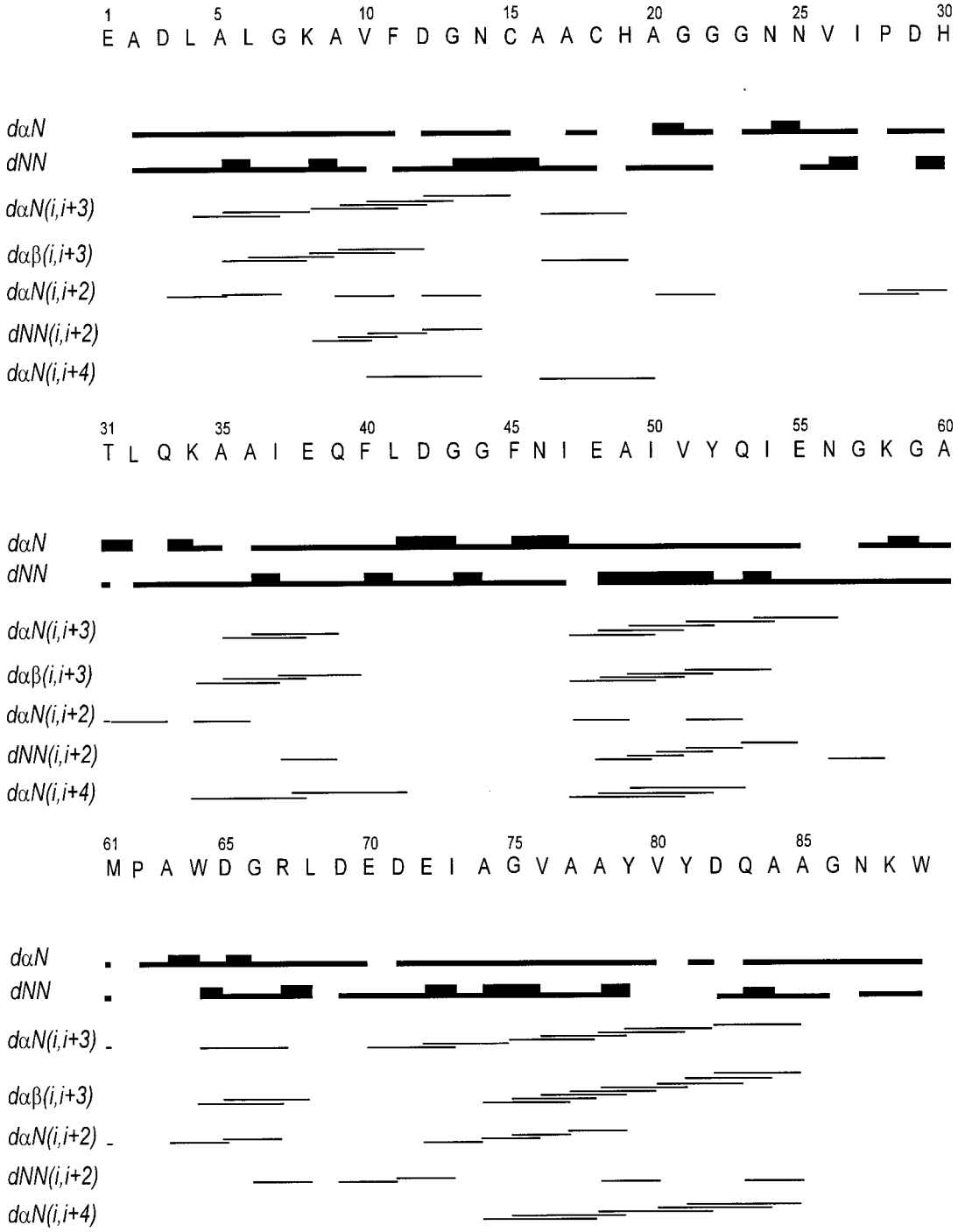

FIGURE 1: Schematic representation of the sequential connectivities involving NH, Hα, and Hβ protons in the oxidized form of cytochrome c_6 from *M. braunii*. For the sequential connectivities, the thickness of the bar indicates the NOE intensities. The medium-range NOEs are identified by lines connecting the two coupled residues.

connectivities, shown in Figure 1, were obtained from the WATERGATE NOESY map with a 100 ms mixing time, recorded in water at 300 K. The NH−NH region of this map is shown in Figure 2.

Sequential NH−NH connectivities for stretches longer than two residues were observed for positions 2−10, 11−18, 19−22, 25−27, 29−31, 32−47, 48−61, 64−68, 69−79, 82−86, and 87 to the C terminus (89). Sequential connectivities have not been observed for the entire protein chain due to the presence of two prolines (Pro28 and Pro62) which do not contain the amide NH. Expected NH−NH connectivities at positions 10, 24, 47, 79−82, and 86 have not been observed because of nearby degenerate amide proton chemical shifts at positions i and $i + 1$. The NH resonance of Gly23 was not found, and therefore, its sequential NH−NH connectivities are not observed. The NH−NH connectivity between residues 31 and 32 has not been detected, due to the long distance between the corresponding protons, which was verified after the structure was solved. The lack of the 68−69 NH−NH connectivity could be due to local mobility which likely occurs in this protein region (later). The absence of the expected NH−NH sequential connectivity between Cys18 and His19 could be explained in terms of severe reduction of NOE intensity, due to the fact they are

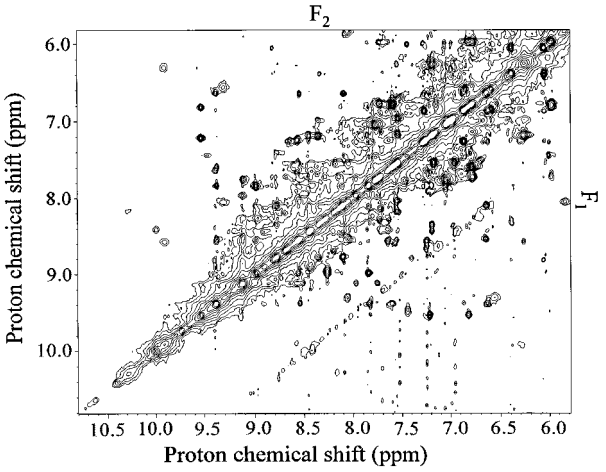

FIGURE 2: NH−NH region of the WATERGATE NOESY spectrum of cytochrome c_6 from *M. braunii* acquired at 500 MHz, 300 K, and pH 5.0 in 10 mM phosphate buffer.

close to the heme. Indeed, as mentioned in the introductory section, the oxidized form is unstable and tends spontaneously to be in the reduced state so that in the sample a small fraction of the reduced protein is often present. The autoreduction of several electron transfer proteins having high reduction potentials is a phenomenon that has been documented for several years and discussed in detail elsewhere (*48*). Addition of potassium ferricyanide often overcomes this problem (*5*, *7*) as it did in the present case. The two oxidation state species of the present protein are exchanging with each other. The heme protons of the oxidized form, which have large hyperfine shifts, have signals that are well separated from those of the reduced form (both of them being observed) and therefore do not experience any broadening due to chemical exchange. On the contrary, for those protons in the vicinity of the heme and which experience smaller shift differences between the oxidized and the reduced forms, this shift separation could be on the order of the exchange rate, thus producing broadening of the lines. Therefore, the connectivities involving these resonances could experience a lower signal-to-noise ratio. As a matter of fact, the total number of dipolar and scalar connectivities is decreased by approximately 10% with respect to the reduced form. When there is no difference in chemical shift between the oxidized and reduced forms, chemical exchange, even if present, cannot produce the above-described effect. A careful search for the conditions for optimal signal detection was performed, and they were found at the pH and ionic strength reported in Materials and Methods.

Sequential Hα−NH dipolar connectivities were found for positions 2−11, 12−15, 17, 18, 20−22, 23−27, 28−35, 36−55, 57−61, 62−70, 71−80, 81 and 82, and 83 to the C terminus (89). For the other residues, Hα−NH connectivities were not detected for the following reasons: the presence of two prolines at positions 28 and 62, the similar chemical shifts of the Hα atoms of two adjacent residues (35 and 36), the location of the Hα resonance under the water signal (Glu55), the inability to detect the Hα (Phe11), and chemical exchange with the reduced form which results in broadening the lines of signals corresponding to protons in the vicinity to the heme Fe(III) ion (15−17 and 56 and 57). This procedure allowed us to perform an almost complete assignment of the ^{1}H NMR resonances in the spectra of the oxidized form of cytochrome c_6 from *M. braunii*. Indeed, 88 amino acids out of 89 were assigned sequence-specifically. The only spin system that was not assigned is that of Glu1. Despite the occurrence of chemical exchange, 84% of the total number of protons have been assigned, which is only 8% less than the corresponding number in the reduced form (where 91% of the total number of protons were assigned). The program GLOMSA provided 34 stereospecific assignments, which were further checked by pseudocontact shift calculations. The complete assignment is available as Supporting Information.

Assignment of the Heme and Its Ligands

The assignment of the resonances of the heme was performed mainly through the NOESY map in D_2O with a 25 ms mixing time, collected in a protein sample containing a small amount (about 5−10%) of the reduced form. In this experiment, very strong EXSY peaks were observed through saturation transfer between the paramagnetically shifted signals of the oxidized form and the corresponding resonances of the reduced form. By taking into account the already published assignment of the heme resonances in the reduced form of cyt c_6 (*18*), we were able to locate the majority of the corresponding resonances in the paramagnetic oxidized form. More specifically, the already published assignment of the heme methyls (1-CH_3, 3-CH_3, 5-CH_3, and 8-CH_3) was confirmed (*17*), and in addition, all meso protons (Hα, Hβ Hγ, and Hδ meso) were identified. The propionate resonances (6-Hα,β and 7-Hα,β) as well as those of the protons and methyls at positions 2 and 4 of the heme ring (2-Hα, 2-βCH_3, 4-Hα, and 4-βCH_3) were identified partially through their EXSY peaks and partially via their NOESY connectivities with the nearby heme methyls and/or meso protons. The Hβ5 side chain and the Hδ1 ring protons of the axial His19 were also identified via saturation transfer. The TOCSY map in H_2O acquired with a 10 ms spin lock time was useful in locating the NH resonance of His19. The spin system of Met61, the other axial ligand to the heme Fe(III), was identified through its observed NOESY sequential connectivities with Ala60, through 1D NOE experiments done on the paramagnetically shifted signal at −8.2 ppm, and through the TOCSY map with a 10 ms mixing time. The resonance at −8.2 ppm, previously tentatively assigned to either one of the Hβ or the Hγ side chain protons of Met61 (*17*), turns out to be the Hγ2 proton of this residue. In addition, for Met61, we have assigned the other Hγ1, one of the Hβ, the Hα, and the NH protons.

Information on the Secondary Structure

Once the backbone and side chain protons were sequence-specifically assigned, the NOESY spectra were examined for medium-range sequential NOEs (Figure 1). Helical structures are characterized by strong sequential NH−NH NOEs and by medium-range backbone (i, $i + 3$) and (i, $i + 4$) NOEs. As shown in Figure 1, Hα−Hβ(i, $i + 3$), Hα−NH(i, $i + 3$), and Hα−NH(i, $i + 4$) connectivities indicated the presence of α-helical motifs for residues 4−14, 16−20, 34−41, 47−56, and 70−85. Backbone (i, $i + 2$) NOEs are observed for 3_{10}-helical elements. With the exception of the segment containing residues 16−20, these kind of NOESY connectivities are observed for several residues involved in

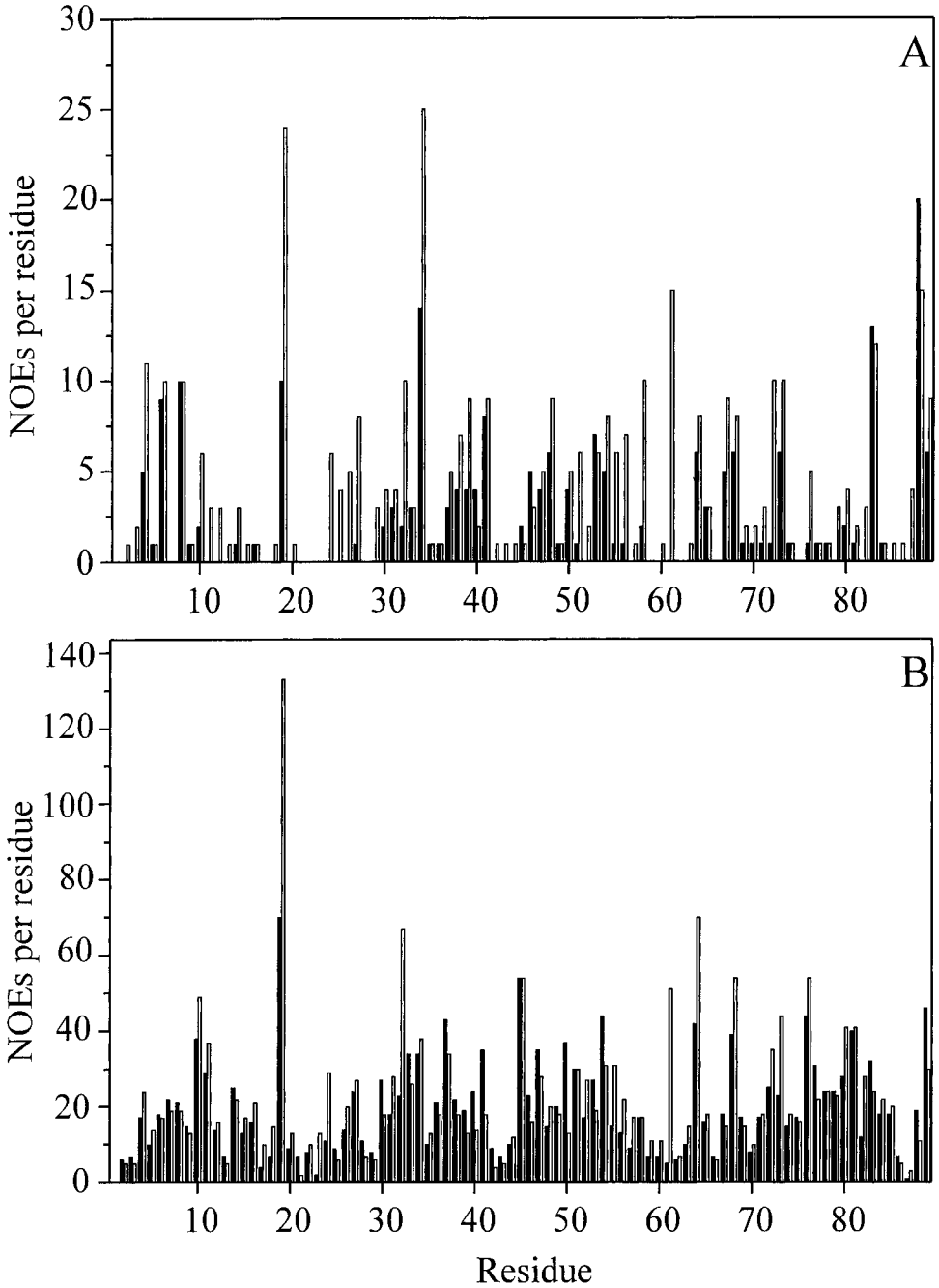

FIGURE 3: Number of intra (A) and inter (B) meaningful NOEs per residue identified in the NMR spectra of reduced (open bars) and oxidized (filled bars) cyt c_6 from *M. braunii*. The total height of each column represents the amount of the observed experimental NOEs. Residue His19 also includes all the heme ring.

the above-mentioned helices, thus suggesting a 3_{10} character for these helices. Analysis of the data reported in Figure 1, therefore, shows that, in close similarity with the reduced form, the main five helical elements are also retained in the oxidized form.

The exchangeable side chain protons of the following residues were identified in the oxidized form: Asn14, Asn24, Asn25, Thr31, Gln33, Asn46, Asn56, Lys58, and Gln83. They all exchange fast with the bulk solvent, and thus, they are undetectable in D_2O.

Solution Structure Determination

NOE Constraints. From the 2D NOESY maps, 1657 experimental constraints were assigned and integrated. Of these, 1533 were found in the NOESY map in H_2O obtained with a 100 ms mixing time, 58 in the equivalent NOESY map in D_2O, and 66 in the NOESY map in D_2O obtained with a 25 ms mixing time. To these, 11 more were added via 1D NOE experiments, thus making a total number of 1668 experimental distance constraints.

Of the 1668 experimental constraints, 1109 were meaningful and therefore have been taken into account by DYANA (and by PSEUDYANA later). The remaining 541 constraints were found to be irrelevant for the calculation (i.e., either no conformation of the polypeptide chain could violate them or they correspond to fixed proton−proton distances). The meaningful NOE constraints per residue are shown in Figure 3 (filled bars), together with the ones of the reduced form

Table 1: rmsd Values (Å) with Respect to the Average Structure (for Families Composed of 40 Structures) Obtained at the Different Levels of Calculations and Evaluated for the Protein Segments Denoted in Parentheses

calculation	DYANA	PSEUDYANA	PSEUDOREM
backbone (3−87)	0.60 ± 0.08	0.59 ± 0.08	0.57 ± 0.08
backbone (7−85)	0.55 ± 0.07	0.51 ± 0.08	0.48 ± 0.08
heavy atoms (3−87)	0.97 ± 0.09	0.96 ± 0.09	0.94 ± 0.09
heavy atoms (7−85)	0.92 ± 0.08	0.89 ± 0.09	0.89 ± 0.08

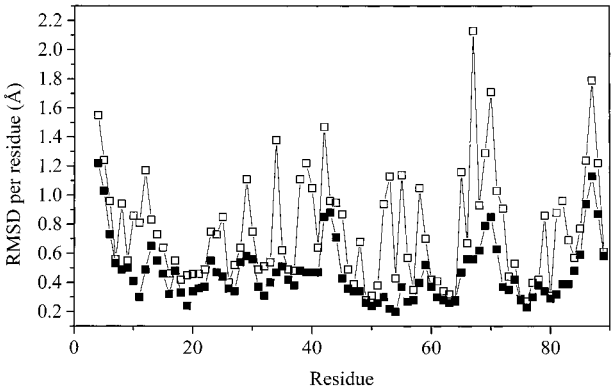

FIGURE 4: rmsd values per residue with respect to the average structure for the PSEUDOREM family of oxidized cyt c_6. rmsd values for the backbone (■) and the heavy atoms (□) are presented.

of the same cytochrome (open bars, taken from ref *18*). In the oxidized form, they correspond to an average of 12.5 accepted experimental constraints per residue. The corresponding number for the reduced form of cytochrome c_6 was 14.5 (*18*). A lower number of NOEs in the oxidized form with respect to the reduced one is particularly observed for the two axial iron ligands (His19 and Met61), for the heme moiety, and for a few other residues (24, 32, and 64). Exchange broadening, due to interconversion between oxidized and reduced forms, could be the main cause for the loss of cross-peaks. At this point, it should be noted that there is an 8% decrease in the number of protons assigned in this work relative to the reduced form of the protein, while the corresponding decrease in the total number of integrated cross-peaks is only 6%. Thus, approximately 2% more NOESY cross-peaks were detected in the spectra of oxidized cytochrome c_6 relative to what would be expected if the same amount of protons had been assigned for both oxidation states of the protein. This slight increase can be accounted for by the more elaborate procedure used in the present work for cross-peak assignment: use of three different 2D NOESY maps, use of 1D NOE experiments, and use of complete relaxation matrix analysis (CORMA) programs to assign extra cross-peaks at the latest stages of the structure calculations (vide infra).

Structure Calculations. Initially, structural calculations were performed by using the program DYANA taking into account 1521 experimental constraints. These resulted in a quite well defined family of 20 structures having rmsd values with respect to the average structure equal to 0.80 ± 0.1 and 1.35 ± 0.11 Å for the backbone and heavy atoms, respectively. At this stage, new NOESY cross-peaks were assigned by using the program CORMA (*37*). Thus, the total number of 1668 experimental constraints was obtained, and new runs of DYANA were performed. Successive runs of the program GLOMSA provided 34 stereospecific assignments. A list of the stereospecific assignments resulting from GLOMSA is available as Supporting Information. The final result of the DYANA calculations was a family of 40 structures with an average target function of 0.68 ± 0.14 Å^2 (lowest, 0.34 Å^2; and highest, 0.87 Å^2). This DYANA family had rmsd values with respect to the average structure equal to 0.60 ± 0.08 and 0.97 ± 0.09 Å for the backbone and heavy atoms, respectively. These numbers account for an already very well defined structure.

To achieve further refinement and to also obtain information on the magnetic properties of the heme, PSEUDYANA calculations were subsequently performed. They were carried out by using the 1668 experimental distance constraints, the 34 stereospecific assignments provided by the program GLOMSA, and in addition 288 pseudocontact shifts. The latter were experimentally determined by subtracting from the shift values of the oxidized form those of the corresponding proton in the reduced form. The shift of geminal protons for which the stereospecific assignment was not available in, at least, one oxidation state was estimated as the difference between the averages of the two oxidation states.

After a few cycles of calculations with the PSEUDYANA program, a family of 40 structures with average total target function of 4.05 ± 0.28 Å^2 (lowest, 3.21 Å^2; and highest, 4.44 Å^2) is obtained. The contributions to the target function are, on average, 1.41 Å^2 for the NOE constraints and 2.64 Å^2 for the pseudocontact shifts. The consistency of the two types of constraints is supported by the fact that the NOE target function does not increase sensibly with respect to calculations performed without the inclusion of pseudocontact shift contraints. A final run of GLOMSA after the end of the PSEUDYANA calculations confirmed all 34 stereospecific assignments of diastereotopic groups. The rmsd values of the PSEUDYANA family with respect to the average structure are 0.59 ± 0.08 and 0.96 ± 0.09 Å for the backbone and the heavy atoms, respectively.

The PSEUDYANA family has been refined through restrained energy minimization (PSEUDOREM) calculations, with the inclusion of the NOE distance and the pseudocontact shifts as constraints. The rmsd values of this final family of 40 structures with respect to the average structure are 0.57 ± 0.08 and 0.94 ± 0.09 Å for the backbone and heavy atoms, respectively. The rmsd values with respect to the average structure for all 40 structure families obtained at the different levels of the calculations are shown in Table 1. The PSEUDOREM calculations converged after six cycles with the axial and rhombic anisotropy components of the magnetic tensor being recalculated after each run. The squared deviations are 0.67 ± 0.09 and 1.95 ± 0.11 Å^2 for the NOE distance constraints and the pseudocontact shift constraints, respectively. In the final family, only 36 calculated pseudocontact shifts deviated more than the tolerance, with 32 of them deviating not more that 0.6 ppm. The four protons with deviations larger than 0.6 ppm are the Hα of residues Leu4 and Glu72, the Hγ of Leu4, and the Hδ1 of Leu68.

The rmsd values per residue for the backbone and heavy atoms within the PSEUDOREM family are shown in Figure 4. The N terminus shows relatively high rmsd values due to the low number of experimental distance constraints (see Figure 3A,B) and also due to the fact that the first residue (Glu1) has not been assigned. Close to the C terminus the

backbone rmsd values show a peak at residue 87 due again to the low number of constraints. The last residue (Trp89) is, however, quite well defined, as it experiences a relatively large number of NOEs. The rmsd values calculated for the average structure of residues 7−85 of the protein are 0.48 ± 0.08 Å for the backbone and 0.89 ± 0.08 Å for the heavy atoms, indicating that the core part of the protein is well defined (see also Table 1). There are three large protein regions which are characterized by rmsd values that are lower than the mean value. These are the fragments 14−41, 45−67, and 72−83 (Figure 4). These fragments are largely involved in α-helix motifs. On the contrary, residues 42−44 and 68−71 are characterized by rmsd values that are higher than those for the whole protein. For the former region, the number of experimental NOE constraints is relatively low, but similar for both oxidation states of cyt c_6. The protein residues in the region of residues 69−72 experience NOEs between the same pairs of protons for the two oxidation states, indicating a similar local conformation. However, for the oxidized form, they have much lower intensity, which then provides interproton distances longer than those for the reduced form (on average larger than 1 Å). This could indicate the presence of local mobility which would then reduce the structure definition. This protein region also contains two protons which experience large violations in the pseudocontact shifts even at the end of the structure calculations. This could be the result of the different effect of mobility on the averaging of the two types of contraints. Indeed, the NOEs depend on $1/r^6$ of short proton−proton distances, while the pseudocontact shifts depend on $1/r^3$ of the iron−proton distance.

The rmsd values per residue for the heavy atoms (Figure 4) are consistently higher than those of the backbone atoms but show the same general trend.

Description of the Structure. The PSEUDOREM family, constituted by 40 structures, is shown in Figure 5. The protein contains four α-helices in the segments 4−14, 34−40, 47−56, and 70−86 as they result from structural analysis performed with the PROCHECK program (*45*). In addition, a short α-helix structure is present for residues 16−20. All these secondary structure elements are consistent with those predicted on the basis of medium-range NOEs. These α-helices are among the best defined parts of the protein, characterized by low rmsd values, due to the presence of interresidue NOEs. Analysis of the structure in terms of ideal geometry shows that 51 residues over a total of 73 "meaningful" residues (non-glycine, non-proline, and non-terminal residues) have φ and ψ dihedral angles which fall in the most favored region (69.9% of the meaningful residues), 18 residues are found in the additionally allowed region (24.6% of the total), and 4 (5.5% of the total) are found in the generously allowed region.

The heme and the iron axial ligands (His19 and Met61) are well defined. Only the carboxylate group of propionate 6 shows some spreading due to less meaningful NOE constraints and nonstereospecific assignment of the Hα and Hβ protons. The projection of the His19 plane on the heme makes an angle of about 15° with the α−γ meso proton direction, toward the NB−ND direction, as also observed in the crystal and solution structures of the reduced form (*18*, *19*). A H-bond between the Nδ1 of His19 and the carbonyl of Gly23 is present, as also found in the structures

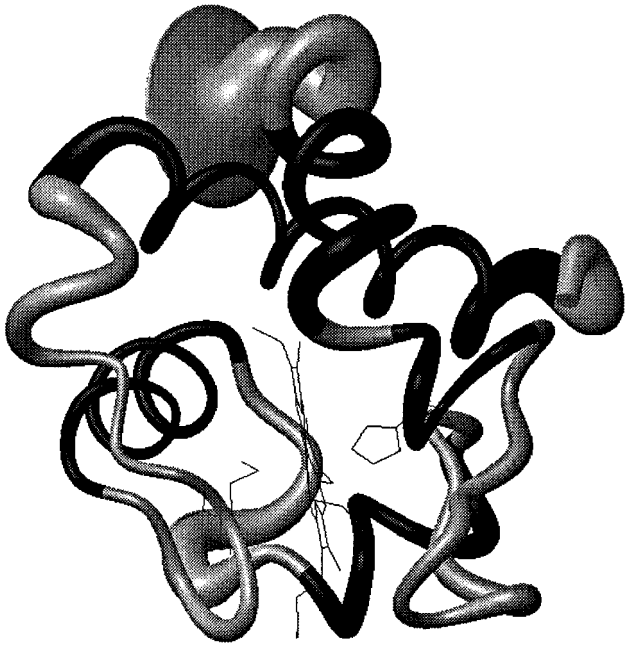

FIGURE 5: Backbone of the PSEUDOREM family of structures for oxidized cyt c_6 from *M. braunii*. The radius of the tube representing the backbone is proportional to the backbone rmsd of the residue. The α-helical parts of the protein are shown with black. The heme ring together with the axial His and Met ligands are also shown. The figure was generated by using the program MOLMOL (*47*).

of the reduced form, which could determine the orientation of the His19 plane, as already proposed (*19*).

The aromatic rings of Phe11, His30, Trp64, and Trp89 are well defined, showing side chain rmsd values of <1.0 Å. The rest of the aromatic rings either are relatively well defined (Tyr81) or are relatively disordered but still have side chain rmsds close to 1.0 Å and constitute a single family (Phe40, Tyr52, and Tyr79).

The protein contains 17 charged residues, 5 of which are positive and 12 of which are negative. All the side chains face toward the solvent, but their degree of disorder differs. Some are well (Glu48 and Asp82) or relatively well (Lys8, Glu38, and Lys88) defined with side chain rmsd values of <1.3 Å. A few others are considerably disordered (Asp3, Arg67, and Glu70) or display two subfamilies (Glu55, Lys34, and Lys58). The six remaining charged residues (Asp12, -29, -42, -69, and -71 and Glu72) show some spreading but constitute a single family in all 40 structures of the PSEUDOREM family.

Magnetic Susceptibility Tensor. The anisotropies of the final tensor are as follows: $\Delta_{ax} = (2.12 \pm 0.02) \times 10^{-32}$ m^3 and $\Delta_{rh} = (0.74 \pm 0.04) \times 10^{-32}$ m^3. The axial χ_{zz} component deviates about 13° from the normal to the mean heme plane. The χ_{xx} and χ_{yy} axes are almost aligned along the Fe−pyrrole nitrogen directions. The first makes an angle of 17.8° with the line of Fe−Nα and the second makes an angle of 11.9° with the line of Fe−Nβ where Nα and Nβ are the pyrrolic nitrogen atoms.

The tensor compares well with those found for other cytochromes with the same iron ligands (*13*, *49*, *50*). Also, the orientations are similar, with the *z* axis deviating 10−15° from the normal to the heme plane and the *x* and *y* directions close to the iron−pyrrole nitrogen bond directions.

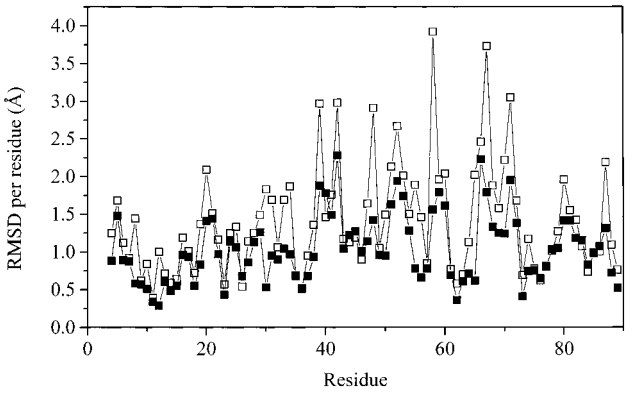

FIGURE 6: rmsd values per residue obtained by sumperimposing the average solution structure of oxidized cyt c_6 with the average solution structure of the reduced form of the same protein. rmsd values for the backbone (■) and the heavy atoms (□) are presented.

Comparison with the Structures of the Reduced Form. To compare the presently determined solution structure of oxidized cyt c_6 with the available structure of the reduced form both in solution (*18*) and in the crystal state (*19*), the use of the average structures in solution (out of a family of 40 structures) was first employed. By superimposing two structures (for example the average solution structure of oxidized cyt c_6 and the average solution structure of reduced cyt c_6) at a time, one can obtain the rmsd values per residue (for both the backbone and the heavy atoms) and thus have a means of quantifying the differences between the two examined structures. While rmsd values of heavy atoms could be relatively high if the side chain is not very well defined within the family, the rmsds for the backbone atoms provide a fairly good measure of the difference between the two examined average structures, since all of these atoms are usually very well defined within each family. To assess the differences and/or similarities of the structures in more detail, a careful inspection of the two families has been conducted by using the program RASMOL (*46*). Thus, it is possible to judge whether the differences obtained by

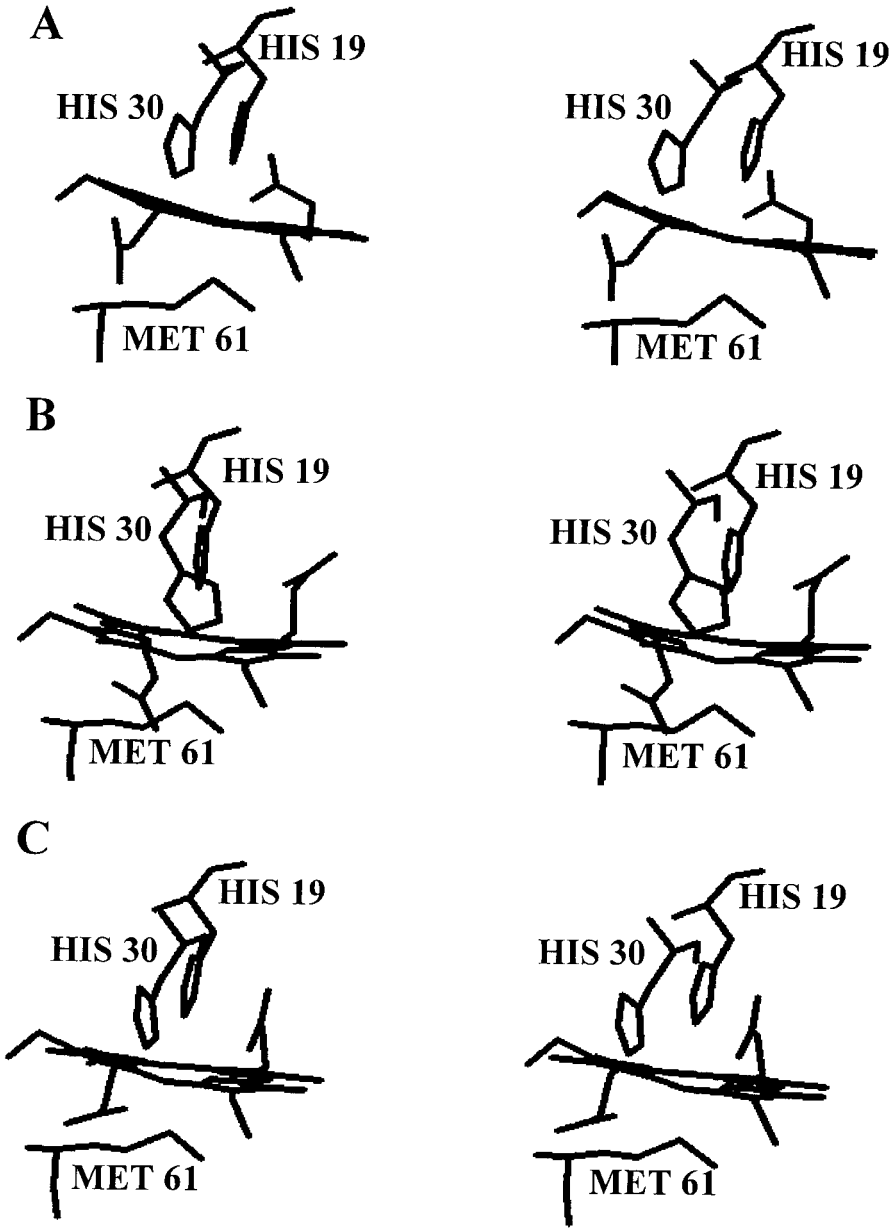

FIGURE 7: Stereodrawing of the conformation of residues 19 (heme ring and axial histidine), 61 (axial methionine ligand), and 30 (histidine) as in the mean structures of the oxidized (A), reduced in solution (B), and reduced in crystal (C) forms of cyt c_6.

comparing only the average structures are real or are just due to poor definition of the examined atoms. In this way, it has been possible to reach definite conclusions regarding side chain conformations. We now proceed with the results of the comparison of the available structures of cyt c_6 by using the methods just described above.

The rmsd values with respect to the average structure obtained for reduced cyt c_6, for a family of 40 structures, were 0.37 ± 0.06 and 0.71 ± 0.05 Å for the backbone and heavy atoms, respectively. The average rmsd value between the average solution structure of reduced cyt c_6 and the X-ray crystal structure is 0.89 Å for the backbone and 1.38 Å for the heavy atoms. The complete comparison of the two available structures of reduced cyt c_6 has already been conducted (*18*). They both are very similar to each other. However, careful examination showed that the side chains of residues 69−72 experience different conformations in the two structures. These residues were proposed to be involved in the recognition of the electron transfer partner and the electron transfer pathway (*51*). In addition, the imidazole ring of His30 in the reduced state of the protein exhibited a different conformation in solution with respect to the X-ray crystal structure. In solution, this residue is located very close to the heme with the exchangeable Hδ1 proton being at an ideal distance and orientation for making a hydrogen bond with a carboxylate oxygen of propionate 7, which has a similar conformation in the two structures. In the solid state, the imidazole ring has moved away and does not form any H bond.

The comparison of the solution structure of cyt c_6 in its oxidized and reduced forms shows that the overall folding of the solution structure of the oxidized form is the same as that of the available structures of the reduced form. The average rmsd value between the average solution NMR structure of oxidized cyt c_6 and the average solution structure of reduced cyt c_6 is 1.14 Å for the backbone and 1.66 Å for the heavy atoms. The rmsd values per residue are reported in Figure 6. These values are small and indicate that the structures are globally quite similar. However, these numbers are larger than the average rmsds obtained within the families of both structures and therefore are indicative of the existence of local meaningful structural differences. The α-helices are formed in the same stretches as in the reduced form. In addition, the other backbone stretches display similar conformations with the exception of residues 39−42, 51−54, 58−60, and 66−72. Furthermore, a few small but consistent differences which can be potentially important for the protein function can be detected for some residues in the protein.

The largest difference between the two structures is the change in the orientation of the Cβ−Cγ bond of propionate 7, which leads to a different orientation of the carboxylate group. Concomitant with this movement, there is a reorientation of His30 and the formation of a H bond between Hδ1 of His30 and one of the two carboxylate oxygens of propionate 7. The comparison between the oxidized and reduced conformations is shown in Figure 7. The conformational change of propionate 7 is experimentally well determined. In the oxidized form, the four protons of this heme substituent experience 14 interresidue NOEs which, among the others, involve connectivities with protons of residues 37 and 41. In the reduced form, propionate 7 experiences fewer interresidue NOEs. However, the change in conformation is clearly revealed by the lack of NOEs with residues 37 and 41, and the presence of NOEs with residue 32. Similarly, the ring of His30 is also quite well defined in the structure of the oxidized cyt c_6, as a consequence of its large number of interresidue NOEs (leading to a heavy atom rmsd value for this residue equal to 0.7 Å in the family composed of 40 structures). In the reduced form, the ring of His30 is characterized by a smaller number of NOEs and shows two subfamilies. They are, however, relatively close each other and sizably different from the conformation of the oxidized form. In addition, the orientation of His30 in the oxidized form is similar to that experienced in the crystal structure of the reduced form. We checked in detail whether the different average orientations experienced in solution by the His30 ring in the two oxidation states of cyt c_6 are well supported by the experimental data. We found that the side chain protons of His30 experience some different long-range NOEs in the two states. In the oxidized state, the side chain protons of His30 give long-range NOEs with the Hαs and the Hβs of propionate 6, with Hβ of Ile27, and with Hβ1 of Asn24, which are not observed in the reduced form. On the contrary, in the reduced form, His30 side chain protons give long-range NOEs with the γ meso of the heme and with Qδ of Ile27, which are not observed in the oxidized form. Furthermore, we checked that all the NOE cross-peaks expected on the basis of the structures have been observed and assigned and that no further cross-peaks were present. We should remember, however, that the two solution structures have been solved at two different pH values, with that of the oxidized form being 5 for stability reasons and that of the reduced being 7, while the crystals were grown at pH 7.5−8. To check the possible effect of pH and/or ionic strength on the above-described structural differences, a NOESY spectrum with a 100 ms mixing time was taken on the reduced form of cyt c_6 at pH 5 and at the same ionic strength as the one used in this work for the oxidized form of cyt c_6. Except for small consistent shifts of the chemical shift values, this map was very similar to the one obtained at pH 7 (*18*) and whose peaks were used for the solution structure determination of reduced cyt c_6. Careful inspection of the NOESY connectivities observed for the four protons of propionate 7 and the side chain protons of His30 showed the presence of the same long-range connectivities with the ones observed in the NOESY map at pH 7 (*18*). Most importantly, the differences in NOEs for these protons between oxidized and reduced cyt c_6 (as described above) also remain at pH 5. Thus, we can safely conclude that the above-described structural differences between the oxidized and reduced forms of cyt c_6 are not merely due to the change of pH or ionic strength.

The crystal structure of reduced cyt c_6 shows (i) the same conformation of the propionate 7 chain as in the solution structure of reduced cyt c_6 and (ii) the same conformation for the His30 ring as in the oxidized solution structure. The fact that three different conformations for the propionate 7−His30 moiety are observed may lead to the conclusion that the differences in energy between these conformations are small and that the energy barrier for the interconversion between them is large with respect to *kT*, as only one conformation is observed through NMR spectroscopy.

A change in the conformation of propionate 7 upon a change in the oxidation state, which in this case also involves

His30, is in accordance with what has already been observed in the solution structures in the two oxidation states of horse heart (*15*, *16*) and yeast (*12*, *13*) cytochromes *c*, although the kind of conformational change is different for the various proteins.

The experimental evidence provided in this work and the references mentioned in the previous paragraph may indicate that propionate 7 has a role in the electron transfer pathway as it reorients itself depending on the oxidation state of the iron and consequently on whether the cytochrome interacts with the oxidant or the reductant. Presumably, the mechanism of molecular recognition in the two cases is different. In the crystal itself, a still different kind of molecular recognition is presumably operating, which leads to the crystallization process.

The acidic patch constituted by residues 69−72 and proposed to be involved in the interaction of cyt c_6 with its redox partners (*51*, *52*) shows some oxidation state-dependent backbone conformational changes even if the structure is less well defined in the oxidized form. As seen in Figure 3, the amount of NOEs for these residues is comparable for both oxidation states of the protein. However, as mentioned before, the intensity of the NOE cross-peaks of this protein region is sizeably reduced in the spectra of the oxidized form. Chemical exchange does not affect NOE intensity, as long as the cross-peaks are detected. This produces an average increase of at least 1 Å for all upper limit distance constraints found in the oxidized versus the reduced state of cyt c_6 for these protein residues. This behavior could justify the lower definition of this part of the protein and could be an indication of local mobility. Despite the larger spreading observed in the oxidized form, the side chains of the first (Asp69) and the last (Glu72) residues show a systematic change in their orientation, with that of Asp69 being larger, with respect to the reduced form. Within the present experimental uncertainty, no significant change is observed for the orientation of the side chains of Glu70 and Asp71. These changes and the local mobility of this protein region might have a role in the free energy interaction with the partner.

Residues Arg67, Trp64, and Tyr52, which have been proposed (*19*) to have a role in the electron transfer pathway, have similar orientations in both forms.

The remaining charged residues have overall similar conformations in both oxidation states with the exception of glutamates 38 and 48 and lysines 8 and 58 which display in all structures of the families the same change in orientation. The side chain of Lys58 is better defined in the oxidized form pointing more toward the heme and specifically closer to propionate 6. In the reduced state, it is more disordered and displays at least two subfamilies of orientation.

The axial ligands of the iron display the same conformation in the two oxidation states, at variance with what is observed in other *c*-type cytochromes (*2*, *8*−*10*, *15*); in particular, His19 does not experience any rotation of its plane, within the present resolution.

With regard to the mechanisms of molecular recognition and redox interactions between cyt c_6 and its redox partners cytochrome *f* and photosystem I (PSI), the structural differences observed between the two redox forms of *M. braunii* cyt c_6 may at least in part account for a change in the affinity for the redox partners. The structural variations herein reported in the heme environment of cyt c_6, in particular those concerning propionate 7 and His30 and in the recognition regions, may have functional implications of some relevance.

CONCLUDING REMARKS

The solution structure of cytochrome c_6 from *M. braunii* in the oxidized paramagnetic form has been obtained. The protein in this state tends to reduce, and its instability does not allow us to perform all the spectroscopic measurements needed for structure determination on the same sample. Furthermore, it causes line broadening, especially for those signals experiencing intermediate hyperfine shifts. Despite these experimental limitations, the solution structure is well resolved with a procedure which uses both NOEs and pseudocontact shifts as structural constraints.

The overall structure is very close to that of the reduced form, although the former is determined at pH 5 and the latter at pH 7. Also, the secondary structure is not altered upon the oxidation state changing. However, the structure of the oxidized form shows that the ring of His30 has a different orientation with respect to that in the solution reduced state, although similar to that in the reduced crystal structure. Associated with the change of the orientation of the His30 ring, a change in the orientation of propionate 7 is observed. The structural changes of propionate 7 which occur in every cytochrome (*12*−*16*) upon redox reaction are rather puzzling. Propionate 7 may have a role in the electron transfer pathway as it would adjust itself to the best conformation to favor the electron uptake and release. The changes in the His30−propionate region may also be a consequence of the interaction of cyt c_6 with PSI and/or with cytochrome *f*.

SUPPORTING INFORMATION AVAILABLE

Table of the assignment of the ^{1}H chemical shifts and the lists of the upper distance limits, the 1D NOE constraints, the pseudocontact shifts used as input for the structure calculations, and the stereospecific assignments resulting from the program GLOMSA (22 pages). Ordering information is given on any current masthead page

REFERENCES

1. Gao, Y., Boyd, J., Pielak, G. J., and Williams, R. J. P. (1991) *Biochemistry 30*, 1928−1934.
2. Berghuis, A. M., and Brayer, G. D. (1992) *J. Mol. Biol. 223*, 959−976.
3. Scott, R. A., and Mauk, A. G., Eds (1996) *Cytochrome c. A multidisciplinary approach*, University Science Books, Sausalito, CA.
4. Banci, L., Bertini, I., Eltis, L. D., Felli, I. C., Kastrau, D. H. W., Luchinat, C., Piccioli, M., Pierattelli, R., and Smith, M. (1994) *Eur. J. Biochem. 225*, 715−725.
5. Bertini, I., Dikiy, A., Kastrau, D. H. W., Luchinat, C., and Sompornpisut, P. (1995) *Biochemistry 34*, 9851−9858.
6. Banci, L., Bertini, I., Dikiy, A., Kastrau, D. H. W., Luchinat, C., and Sompornpisut, P. (1995) *Biochemistry 34*, 206−219.
7. Bertini, I., Eltis, L. D., Felli, I. C., Kastrau, D. H. W., Luchinat, C., and Piccioli, M. (1995) *Chem.−Eur. J. 1*, 598−607.
8. Louie, G. V., and Brayer, G. D. (1990) *J. Mol. Biol. 214*, 527−555.
9. Takano, T., and Dickerson, R. E. (1981) *J. Mol. Biol. 153*, 95−155.
10. Takano, T., and Dickerson, R. E. (1981) *J. Mol. Biol. 153*, 79−94.

11. Berghuis, A. M., Guillemette, J. G., McLendon, G., Sherman, F., Smith, M., and Brayer, G. D. (1994) *J. Mol. Biol. 236*, 786−799.
12. Baistrocchi, P., Banci, L., Bertini, I., Turano, P., Bren, K. L., and Gray, H. B. (1996) *Biochemistry 35*, 13788−13796.
13. Banci, L., Bertini, I., Bren, K. L., Gray, H. B., Sompornpisut, P., and Turano, P. (1997) *Biochemistry 36*, 8992−9001.
14. Qi, P. X., Beckman, R. A., and Wand, A. J. (1996) *Biochemistry 35*, 12275−12286.
15. Banci, L., Bertini, I., Gray, H. B., Luchinat, C., Reddig, T., Rosato, A., and Turano, P. (1997) *Biochemistry 36*, 9867−9877.
16. Qi, P. X., Di Stefano, D. L., and Wand, A. J. (1994) *Biochemistry 33*, 6408−6417.
17. Campos, A. P., Aguiar, A. P., Hervás, M., Regalla, M., Navarro, J. A., Ortega, J. M., Xavier, A. V., De la Rosa, M. A., and Teixeira, M. (1993) *Eur. J. Biochem. 216*, 329−341.
18. Banci, L., Bertini, I., Quacquarini, G., Walter, O., Diaz, A., Hervás, M., and De la Rosa, M. A. (1996) *JBIC, J. Biol. Inorg. Chem. 1*, 330−340.
19. Frazao, C., Soares, C. M., Carrondo, M. A., Pohl, E., Dauter, Z., Wilson, K. S., Hervás, M., Navarro, J. A., De la Rosa, M. A., and Sheldrick, G. (1995) *Structure 3*, 1159−1170.
20. Macura, S., Wüthrich, K., and Ernst, R. R. (1982) *J. Magn. Reson. 47*, 351−357.
21. Marion, D., and Wüthrich, K. (1983) *Biochem. Biophys. Res. Commun. 113*, 967−974.
22. Bax, A., and Davis, D. G. (1985) *J. Magn. Reson. 65*, 355−360.
23. Griesinger, C., Otting, G., Wüthrich, K., and Ernst, R. R. (1988) *J. Am. Chem. Soc. 110*, 7870−7872.
24. Bax, A., Freeman, R., and Morris, G. (1981) *J. Magn. Reson. 42*, 164−168.
25. Bax, A., and Freeman, R. (1981) *J. Magn. Reson. 44*, 542−561.
26. Piotto, M., Saudek, V., and Sklenar, V. (1992) *J. Biomol. NMR 2*, 661−666.
27. Satterlee, J. D., and Erman, J. E. (1991) *Biochemistry 30*, 4398−4405.
28. Satterlee, J. D., Erman, J. E., and de Ropp, J. S. (1987) *J. Biol. Chem. 262*, 11578−11583.
29. Banci, L., Bertini, I., Luchinat, C., Piccioli, M., Scozzafava, A., and Turano, P. (1989) *Inorg. Chem. 28*, 4650−4656.
30. Eccles, C., Güntert, P., Billeter, M., and Wüthrich, K. (1991) *J. Biomol. NMR 1*, 111−130.
31. Güntert, P., Braun, W., and Wüthrich, K. (1991) *J. Mol. Biol. 217*, 517−530.
32. Wüthrich, K. (1989) *Acc. Chem. Res. 22*, 36−44.
33. Güntert, P., and Wüthrich, K. (1991) *J. Biomol. NMR 1*, 447−456.
34. Bertini, I., Felli, I. C., Luchinat, C., and Rosato, A. (1996) *Proteins: Struct., Funct., Genet. 24*, 158−164.
35. Bertini, I., Luchinat, C., and Rosato, A. (1996) *Prog. Biophys. Mol. Biol. 66*, 43−80.
36. Banci, L., Bertini, I., Bren, K. L., Gray, H. B., Sompornpisut, P., and Turano, P. (1995) *Biochemistry 34*, 11385−11398.
37. Borgias, B., Thomas, P. D., and James, T. L. (1989) *Complete Relaxation Matrix Analysis (CORMA)*, University of California, San Francisco.
38. Bentrop, D., Bertini, I., Cremonini, M. A., Forsén, S., Luchinat, C., and Malmendal, A. (1997) *Biochemistry 36*, 11605−11618.
39. La Mar, G. N., Horrocks, W. D. W., and Holm, R. H., Eds. (1973) *NMR of Paramagnetic Molecules*, Academic Press, New York.
40. Bertini, I., and Luchinat, C. (1996) *Coord. Chem. Rev. 150*.
41. Banci, L., Bertini, I., Bren, K. L., Cremonini, M. A., Gray, H. B., Luchinat, C., and Turano, P. (1996) *JBIC, J. Biol. Inorg. Chem. 1*, 117−126.
42. Banci, L., Bertini, I., Gori Savellini, G., Romagnoli, A., Turano, P., Cremonini, M. A., Luchinat, C., and Gray, H. B. (1997) *Proteins: Struct., Funct., Genet. 29*, 68−76.
43. Pearlman, D. A., and Case, D. A. (1991) *SANDER*, University of California, San Francisco.
44. Pearlman, D. A., Case, D. A., Caldwell, J. W., Ross, W. S., Cheatham, T. E., Ferguson, D. M., Seibel, G. L., Singh, U. C., Weiner, P. K., and Kollman, P. A. (1995) *AMBER 4.1*, University of California, San Francisco.
45. Laskowski, R. A., MacArthur, M. W., Moss, D. S., and Thornton, J. M. (1993) *J. Appl. Crystallogr. 26*, 283−291.
46. Sayle, R. (1994) *RASMOL*, Biomolecular Structure Department, Glaxo Research and Development, Greenford, Middlesex, U.K.
47. Koradi, R., Billeter, M., and Wüthrich, K. (1996) *J. Mol. Graphics 14*, 51−55.
48. Bartsch, R. G. (1978) in *The photosynthetic bacteria* (Clayton, R. K., and Sistrom, W. R., Eds.) pp 249−279, Plenum Press, New York.
49. Emerson, S. D., and La Mar, G. N. (1990) *Biochemistry 29*, 1556−1566.
50. Turner, D. L., and Williams, R. J. P. (1993) *Eur. J. Biochem. 211*, 555−562.
51. Hervás, M., Navarro, J. A., Diaz, A., and De la Rosa, M. A. (1996) *Biochemistry 35*, 2693−2698.
52. Hervás, M., Navarro, J. A., Diaz, A., Bottin, H., and De la Rosa, M. A. (1995) *Biochemistry 34*, 11321−11326.

BI972765Y